Beyond the Nearest-Neighbor Zimm–Bragg Model for Helix-Coil Transition in Peptides

Adrian Murza,* Jan Kubelka
Chemistry Department 3838, University of Wyoming, 1000 E University Ave., Laramie, WY, 82072

Received 7 July 2008; revised 14 September 2008; accepted 15 September 2008
Published online 23 September 2008 in Wiley InterScience (www.interscience.wiley.com). DOI 10.1002/bip.21093

ABSTRACT:

The nearest-neighbor ($\mu = 1$) variant of the Zimm and Bragg (ZB) model has been extensively used to describe the helix-coil transition in biopolymers. In this work, we investigate the helix-coil transition for a 21-residue alanine peptide (AP) with the ZB model up to fourth nearest neighbor ($\mu = 1$, 2, 3, and 4). We use a matrix approach that takes into account combinations of any number of helical stretches of any length and therefore gives the exact statistical weight of the chain within the assumptions of the ZB model. The parameters of the model are determined by fitting the temperature-dependent circular dichroism and Fourier transform infrared experimental spectra of the AP. All variants of the model fit the experimental data, thus giving similar results in terms of the macroscopic observables, such as temperature-dependent fractional helicity. However, the resulting microscopic parameters, such as distributions of the individual residue helical probabilities and free energy surfaces, vary significantly depending on the variant of the model. Overall, the mean residue enthalpy and entropy (in the absolute value) both increase with μ, but combined yield essentially the same "effective" value of the ZB propagation parameters for all μ. Greater helical probabilities for individual residues are predicted for larger μ, in particular, near the center of the sequence. The ZB nucleation parameters increase with increasing μ, which results in a lower free energy barrier to helix nucleation and lower apparent "cooperativity" of the transition. The significance of the long-range interactions for the predictions of ZB model for helix-coil transition, the calculated model parameters and the limitations of the model are discussed. © *2008 Wiley Periodicals, Inc. Biopolymers 91: 120–131, 2009.*

Keywords: Zimm–Bragg model; helix-coil transition; alanine peptide

This article was originally published online as an accepted preprint. The "Published Online" date corresponds to the preprint version. You can request a copy of the preprint by emailing the Biopolymers editorial office at biopolymers@wiley.com

INTRODUCTION

Transition between the α-helical structures and random coil is one of the important elementary steps in folding of polypeptide chains into functional proteins. Following the early observations of cooperative helix to random coil transitions in polypeptides,[1,2] a family of simple statistical mechanical treatments for the helix-coil equilibria was developed.[3] All these models have in common that the polypeptide chains are represented as one-dimensional sequences of linked amino acid residues, where each of the individual residues can exist in one of only two possible states: helix or coil. Such simple representation allows calculating the partition functions and therefore the thermodynamic parameters for the helix-coil transition in terms of very few parameters that can be obtained from the experimental data. With the discovery of stable alanine-rich oligopeptides as models for the α-helices in proteins,[4] the he-

**Present address:* IFISC, Instituto de Física Interdisciplinar y Sistemas Complejos (CSIC-UIB), E-07122 Palma de Mallorca, Spain.
Correspondence to: Chemistry Department 3838, University of Wyoming, 1000 E University Ave., Laramie, WY, 82072; e-mail: jkubelka@uwyo.edu

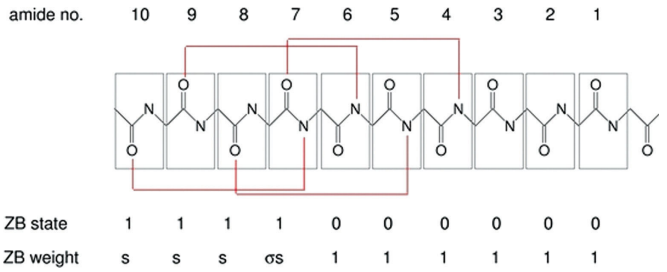

SCHEME 1 Hydrogen bonding in the α-helix with Zimm–Bragg notation and weighing scheme.

lix-coil transition received a renewed interest[5–9] and the statistical mechanical models for helix-coil transition have been extended to include additional interactions.[5,9]

One of the most popular statistical mechanical models for the helix-coil transitions is the Zimm–Bragg (ZB) model.[10] The ZB model assumes that a given state of the chain can be completely described by the hydrogen bonding state of the amide oxygen atoms; that is whether or not each oxygen is hydrogen bonded to the amino group of the third preceding segment (Scheme 1). The equilibrium constant for transforming a coil residue into a helical residue at the end of a helical sequence is given by the propagation parameter s, which corresponds to the equilibrium constant between the helix and coil state of the last residue and is on the order of unity. The equilibrium constant for initiating a helical unit is given by σs, where σ is much smaller than one and is known as the nucleation parameter.

Because of its simplicity, the most commonly used variant of the ZB model is the nearest neighbor ($\mu = 1$), in which the statistical weight of the state of each amide group depends only on the state of the preceding one.[6,10–12] Since there are ~3.6 residues per α-helical turn and a hydrogen bond is formed between the residues i and $i + 4$ (amide groups i and $i + 3$, Scheme 1), the ZB model which considers interactions between segments formed by three successive amide groups ($\mu = 3$) has been generally considered most appropriate for characterizing the helix-coil transition.[3,6,10] However, μ does not represent the range of hydrogen bonding, which is always assumed to occur to the third preceding segment, but an effective "cutoff" for the decrease in the statistical weight due to a hydrogen bond following a stretch of unbonded segments.[10] As a consequence, it is not obvious which value of μ would give the most realistic description of the helix-coil transition.

A number of extensions of the nearest-neighbor ZB approach, which include specific side chain interactions,[13–16] and modified models with additional parameters were proposed.[16,17] Wako et al.[18] presented a rigorous statistical mechanical treatment of the polypeptide chain with interactions up to the fourth nearest neighbor and applied it to analysis of the α-helical and extended segments in proteins. This model[3,19,20] is similar to ZB, but the interresidue interactions are taken into account explicitly with additional interaction terms and the application to protein sequences also explicitly accounted for residue-specific interactions. The important result of the Wako et al. study[18] was that the long range interactions (up to $\mu = 4$ in our notation) were necessary to reproduce the correct experimental protein conformation.

The objective of this work is to systematically investigate the effects of incorporating the long-range interactions in the ZB model[10] on the analysis of helix-coil transition in a model oligopeptide. We adhere to the original formulation of the model, which only considers intrahelical hydrogen bonding but does not take into account the heteropolymer nature of the peptide by explicitly including any specific residue-dependent interactions as the model of Wako et al.[18] Within the assumptions of the ZB model we obtain the exact solution for the statistical weight of the chain by taking into account combinations of any number of helical stretches of any length. This is in contrast to simplifying assumptions that are often made, such as a single sequence approximation, which allow only a single helical stretch.[6,7,9,10] The four ($\mu =$ 1, 2, 3, and 4) variants of the model are used to describe the helix-coil transition in an alanine-rich peptide, measured experimentally by circular dichroism (CD) and Fourier transform infrared (FTIR) spectroscopy. The different variants of the ZB model are compared in terms of the microscopic parameters, such as conformational free energies and residue helical probabilities, which are obtained from the best fit to the experimental data. We also use these parameters to calculate and compare the microscopic distributions of the helical probabilities within the oligopeptide chain as well as the free energy surfaces for the helix-coil transition. Finally, we discuss the implications of the long-range interactions on the microscopic predictions of the ZB model along with important limitations of the model.

EXPERIMENTAL

Peptide Synthesis

The 21-residue oligopeptide with the sequence Ac-AAAAAAAAR-AAAARAAAARAA—COOH (denoted AP) was synthesized using standard FMOC solid phase synthesis methods on a PS3 peptide synthesizer (Protein Technologies Inc.). The synthesized peptide was purified by HPLC to >95% purity as evidenced by MALDI-TOF mass spectrometry.

Experimental Measurements

Far-ultraviolet CD spectra were recorded from 260 to 180 nm on a Jasco-810 spectropolarimeter, equipped with a thermoelectric

(Peltier) device for precise temperature control. The samples were prepared at 300 μM peptide concentration in water at pH 7 and measured in a 0.2-cm pathlength quartz cuvette. The pH of the samples was adjusted to pH 7 by adding minute amounts of aqueous NaOH solution. The temperature-dependent spectra were recorded from 273 to 348 K with a step of 5 K. The CD spectra were acquired in the continuous mode with 1-nm bandwidth, 1-s response, and a scan speed of 20 nm min^{-1}; 16 scans were accumulated to obtain the final spectra. The CD baseline was corrected by subtracting identically measured CD traces of just the water.

The FTIR absorption spectra were recorded using a Bruker Tensor 27 (FTIR) spectrometer, equipped with a RT-DLaTGS detector, at 4 cm^{-1} nominal resolution. The samples were prepared in D_2O at 20 mg mL^{-1} peptide concentration at pH 7. An average of 256 scans was collected every 5 K from 273 to 318 K. The temperature was controlled by an external water bath connected to the heating jacket/sample cell assembly (Specac). The sample cell consisted of CaF_2 windows and 50-μm Teflon spacer. The exact temperature of the sample was measured with a thermocouple. The FTIR baseline was corrected by subtracting identically measured FTIR traces of just D_2O.

CALCULATIONS

All calculations were carried out using Matlab (Mathworks, Inc). Below we outline the Zimm–Bragg theory, the matrix method and its extensions employed for calculations of the partition functions as well as the procedures used to find the parameters by fitting the experimental data.

Zimm–Bragg Model

In the ZB formalism, each amide unit of the peptide chain can assume one of two possible configurations: hydrogen bonded on the amide C=O, denoted as "1" or unbonded "0" (Scheme 1). For shortness, we will also call the hydrogen-bonded residues "helical" and the unbonded ones "coil". The partition function for the oligopeptide chain is the sum of the statistical weights of individual configurations, which are constructed as the product of the following four factors:[10]

1 The quantity unity for every 0 (unbonded segment);
2 The quantity s for every 1 that follows another 1 (bonded segment);
3 The quantity σs for every 1 that follows μ or more 0s;
4 The quantity 0 for every 1 that follows a number of 0's less than μ.

The propagation factor s measures the contribution to the partition function of a bonded residue relative to that of an unbonded residue and can be expressed in terms of the enthalpy (ΔH) and entropy (ΔS) changes due to adding a bonded residue:

$$s = \exp[-(\Delta H - T\Delta S)/RT] \tag{1}$$

The nucleation factor σ is used to describe the large decrease in the statistical weight caused by the first bond after μ or more unbonded residues; it is assumed independent of temperature. The quantity μ represents the range of the interresidue interaction, whereby the state of each particular segment (amide group) depends on the states of μ preceding segments. Thus, $\mu = 1$ corresponds to the nearest-neighbor interactions only, $\mu = 2$, 3, and 4 take into account the interactions up to the second, third, and fourth nearest neighbors, respectively.

The Matrix Method

The partition function Q for the peptide chain can be enumerated exactly using the matrix formalism:[10]

$$Q = \omega \mathbf{M}^{\mathbf{n}+\mu-\mathbf{4}} \alpha^{\dagger} \tag{2}$$

where $\boldsymbol{\alpha} = (1,0,0,\ldots,0)$ and $\boldsymbol{\omega} = (1,1,1,\ldots,1)$ are vectors of length 2^{μ}, $\mathbf{M}$ is a $2^{\mu} \times 2^{\mu}$ matrix and n is the length of the chain. The explicit forms of the matrices $\mathbf{M}$ for $\mu = 1$, 2, 3, and 4 are given in the Appendix. Equation (2) ensures that the first three residues of the chain are always "coil" (i.e., nonhydrogen bonded). Calculation of the partition function, therefore, reduces into multiplications of the statistical weight matrices $\mathbf{M}$.

The earlier formalism also allows calculations of the states of the individual segments. The probability that segment i is in joint configuration l is given by:

$$p_i(l) = b_{i,l} a_{i,l} / Q \tag{3}$$

where,

$$\mathbf{a}_i^{\dagger} = \mathbf{M}^{\mathrm{i}+\mu-4} \alpha^{\dagger} \tag{4}$$

$$\mathbf{b}_i = \omega \mathbf{M}^{n-i} \tag{5}$$

are statistical weight vectors, whose components are the aggregate statistical weights of the possible joint configurations of the part of the chain preceding ($\mathbf{a}_i$) and following ($\mathbf{b}_i$) the segment of interest. Obviously, $\mathbf{b}_i \cdot \mathbf{a}_i^{\dagger} = \mathbf{Q}$.

Calculations of Average Fractional Helicity

The matrix formalism can be used to calculate the partition function as well as the probabilities that the individual amino acid residues in the chain are helical (or, strictly speaking, hydrogen bonded on C=O). However, it is not entirely straightforward to express the probability for the overall fraction of the helical residues irrespective of the residue position. Since the overall average helical content is measured

experimentally, this quantity is necessary for fitting the experimental data. To calculate the probability of the configurations with given number of helical residues, we decompose the partition function as follows:[21]

$$Q = 1 + \sum_{q=1}^{n-3} Q_q \lambda^q \tag{6}$$

where Q_q is the partition function of all the configurations with the q helical residues and λ is a dummy variable, which multiplies each hydrogen-bonded (helical) state (i.e., s and σs) in the statistical weight matrices. Therefore, the exponent of λ tracks the number of helical residues. The probability of the configuration with q helical residues is then given as:

$$p(q) = \frac{Q_q}{Q} = \exp(-\Delta G_q / RT) \tag{7}$$

where ΔG_q is the Gibbs free energy of the particular configuration with respect to the all-coil state. Equation (7) can also be used to calculate free energy surfaces as a function of the fraction of the helical residues representing the reaction coordinate. The fractional helicity θ_T at a specified temperature T is then:

$$\theta_T = \frac{1}{n} \sum_{q=1}^{n-3} q p(q) \tag{8}$$

Modeling the Experimental Data

The sets of experimental CD and FTIR temperature-dependent data were first decomposed by singular value decomposition (SVD):[22]

$$\mathbf{D} = \mathbf{USV}^{\mathbf{T}} = \mathbf{UC}^{\mathbf{T}} \tag{9}$$

where **U** is the matrix of the basis functions (spectra), **V** is the matrix of temperature-dependent coefficients, and **S** is the diagonal matrix of the singular values. We denote as **C** the matrix of the coefficients contracted with the corresponding singular values **S**: **C** = **VS**. Two significant components for each set of data were retained and simultaneously fitted to the fractional populations of helix θ_T and coil states $(1 - \theta_T)$, obtained from the ZB model [Eq. (8)]. With a given set of parameters ΔH, ΔS, and s, first the linear fitting procedure is used to find the combination of **C** vectors that gives the best least squares fit to the populations. The parameters are then varied and the earlier procedure repeated until the sum of squares is then minimized.

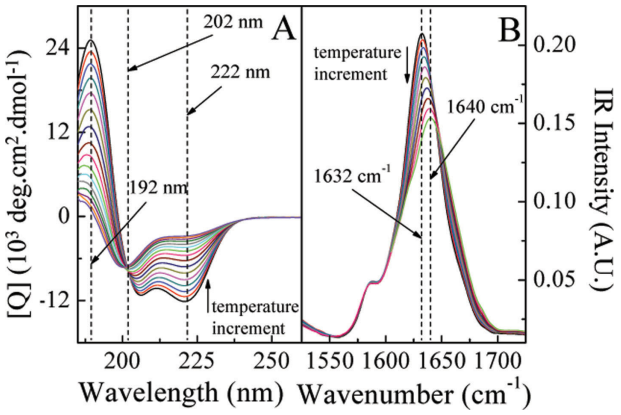

FIGURE 1 Experimental data for the helix-coil transition in the alanine 21-mer peptide (AP). Temperature-dependent CD (A) amide I' FTIR (B) for the AP from 273 to 318 K every 5 K.

RESULTS

Experimental Data Analysis and Parameters of the Model

Temperature-dependent far-ultraviolet CD and amide I′ FTIR spectra of AP are shown in Figure 1. The CD spectra of the AP (Figure 1A) are characterized by a deep (negative) minimum at 222 nm and a secondary minimum at 208 as well as a maximum at 192 nm typical for the α-helical conformation. The 222 and 208 nm CD increases with the increasing temperature while the 192 nm maximum decreases, indicating the α-helix to random coil transition of the AP. The highest temperature CD (at 248 K) has a pronounced minimum around 200 nm, but preserves some negative ellipticity at 222 nm as well as positive at 192 nm, indicating that even at 248 K the peptide is not fully random coil. Figure 1A shows a well defined isodichroic point at 202 nm, which is often regarded as a signature for just two states in the system.

The helix-coil transition in the AP is also monitored by the frequency and intensity changes in the amide I′ FTIR spectrum (Figure 1B). The amide I′ peak frequency shows a shift from 1633 cm^{-1} at 273 K to 1640 cm^{-1} at 318 K, which is characteristic for helix-coil transition in alanine-rich oligopeptides.[23–25] In addition, the peak intensity of the amide I′ decreases and the band broadens with the increasing temperature, again reflecting the melting of the regular α-helical structure into the random coil.

In many cases, CD ellipticity at 222 nm and the FTIR amide I′ band frequencies are used to estimate the α-helical content. We used a more general approach, which does not reduce the experimental spectra into a single frequency or intensity changes, but takes into account all the features of the CD and FTIR experimental spectra. SVD of the spectral sets

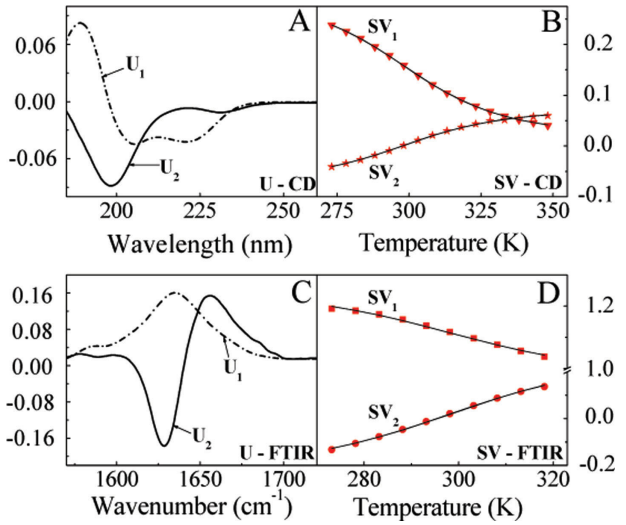

FIGURE 2 Singular value decomposition (SVD) and global fitting analysis of the experimental data. Basis spectra (columns of U) from the SVD of the CD (A). First component is shown as a dashed line, second as a solid line. Corresponding temperature-dependent coefficients (columns of V weighted by the singular values) for the first (red triangles) and second (red stars) component, along with the fit (black lines) to the $\mu = 1$–4 variants of ZB model (B). (The curves from individual ZB model variants are superimposable.) FTIR basis spectra for the first (dashed) and second (solid) SVD components (C). Corresponding temperature-dependent first (red squares) and second (red circles) component SV vectors (**D**). The fits to the four variants of the ZB model are shown as black lines.

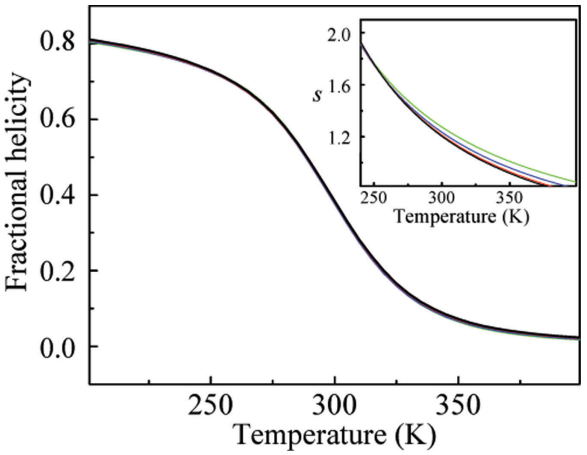

FIGURE 3 Fractional helicity (fraction of intersegment hydrogen bonds) θ_T as a function of temperature for the four variants of ZB model: $\mu = 1$ (green), $\mu = 2$ (blue), $\mu = 3$ (red) and $\mu = 4$ (black). Inset: temperature dependence of the propagation parameter s for $\mu = 1$ (green), $\mu = 2$ (blue), $\mu = 3$ (red) and $\mu = 4$ (black).

provides basis for such global analysis of the experimental data sets.[22] SVD of the experimental CD and amide I′ FTIR spectra of the AP yielded two significant components for each data set, that is, two **U** and **V** eigenvectors corresponding to the highest and second-highest singular values **S**, which accounted for >99% of the data. The remaining components contain only noise and were discarded.

The results of the SVD, the basis spectra **U** and the weighted temperature-dependent coefficients **C** [Eq. (9)] are shown in Figure 2 along with the best fits to the four variants ($\mu = 1$, 2, 3, and 4) of the ZB model. The fitting was performed as described earlier (see "Calculations" section), using the full matrix representation of the $\mu = 1$, 2, 3, and 4 ZB model to obtain the populations of "helix" and "coil" states. The resulting fractional helical populations (or, rigorously, the fractions of the hydrogen bonds formed) are shown in Figure 3. The inset in Figure 3 shows the dependence of the propagation parameter s [Eq. (1)] on temperature.

From Figure 3, it is evident that the overall population of the helical states is the same independently of the particular variant of the model. This is a consequence of fitting to the same set of the experimental CD and FTIR data, which monitor the overall α-helical content. As a result of the ZB postulate that the first three residues in the chain are invariably hydrogen unbonded (i.e., "coil"), the maximum helical content of a 21-residue peptide is 18/21 ≈ 85%. The curves in Figure 3 approach this value in the limit of very cold temperature. For high temperatures, the peptide becomes random coil, and the average helical content converges to zero.

The resulting parameters from the best fits of the individual variants of the model are summarized in Table I. The enthalpy and entropy values, as well as the nucleation parameters (Table I) fall within the range of previously determined values for helix-coil transition in alanine-rich oligopeptides.[5,14,26–33] On the other hand, the parameters are significantly different from those determined by Scheraga and coworkers from studies on triblock[34] and host–guest random[35] copolymers. These differences are likely to arise from our treatment of the oligopeptides, which are effectively copolymers, as homopolymers and mainly from our neglect of the effect of the charged residues (in our case Arg) on the pep-

Table I Parameters of the Four Variants of the Zimm-Bragg Model ($\mu = 1$–4) Obtained from the Best Fit of the Experimental CD and FTIR data

μ	σ ($\times 10^{-3}$)	ΔH (cal mol^{-1} res^{-1})	ΔS (cal mol^{-1} K^{-1} res^{-1})
1	(1.4 ± 0.1)	−978 ± 9	−2.78± 0.02
2	(2.3 ± 0.2)	−1044 ± 10	−3.06± 0.03
3	(3.2 ± 0.3)	−1100 ± 10	−3.28± 0.03
4	(3.9 ± 0.3)	−1133 ± 10	−3.41± 0.03

Table II Mean Values and Standard Deviations of Temperature-Dependent Propagation Parameters Corresponding to ($\mu = 1$–4) Shown as an Inset of Figure 3

T (K)	$\mu = 1$	$\mu = 2$	$\mu = 3$	$\mu = 4$
273	1.49 ± 0.03	1.47 ± 0.03	1.45 ± 0.04	1.45 ± 0.04
300	1.27 ± 0.02	1.23 ± 0.03	1.21 ± 0.03	1.20 ± 0.03
328	1.10 ± 0.02	1.06 ± 0.02	1.04 ± 0.02	1.02 ± 0.02
348	1.01 ± 0.02	0.97 ± 0.02	0.94 ± 0.02	0.92 ± 0.02

tide backbone solvation.[36–38] We will return to these values in the "Discussion" section, here we only point out that our goal is not the accurate determination of the helix-coil transition parameters, but comparison of different variants of ZB model.

The (microscopic) parameters of the model differ significantly, depending on the value of μ: the nucleation parameter σ increases with the increasing μ as do, in the absolute value, the enthalpy and entropy changes per residue for the helix propagation (Table II). Interestingly, the resulting propagation parameters s (see Figure 2), also listed for several temperatures in Table III, are very similar for all μ, despite the variation in ΔH and ΔS. In fact, at low temperatures, where the peptide is mostly helical, within error the s values are the same for all μ (Table III). At higher temperatures (T $\gtrsim$ 300 K) the propagation parameters become smaller for higher μ.

Helical Probability Distributions for Individual Residues

The probabilities that a residue is helical (hydrogen bonded) for the $\mu = 1$, 2, 3, and 4 variants of the ZB model have been calculated from Eq. (3) and are shown in Figure 4 for two temperatures, 273 K (Figure 4A), and 300 K (Figure 4B). These temperatures were chosen because high α-helical content is observed at 273 and at 300 K a substantial fraction of AP α-helix is converted into random coil, highlighting the temperature-dependent residue helical probabilities.

Table III The Nucleation Free-Energy Barrier for the Four Variants of the ZB Model ($\mu = 1$–4) at Several Temperatures

	Nucleation Free Energy Barrier (kcal mol^{-1})			
T (K)	$\mu = 1$	$\mu = 2$	$\mu = 3$	$\mu = 4$
273	1.81 ±0.03	1.54 ±0.04	1.34 ±0.03	1.27 ±0.03
300	2.08 ±0.04	1.79 ±0.04	1.58 ±0.04	1.49 ±0.04
328	2.37 ±0.04	2.06 ±0.05	1.84 ±0.04	1.76 ±0.04
348	2.58 ±0.04	2.25 ±0.05	2.02 ±0.04	1.93±0.04

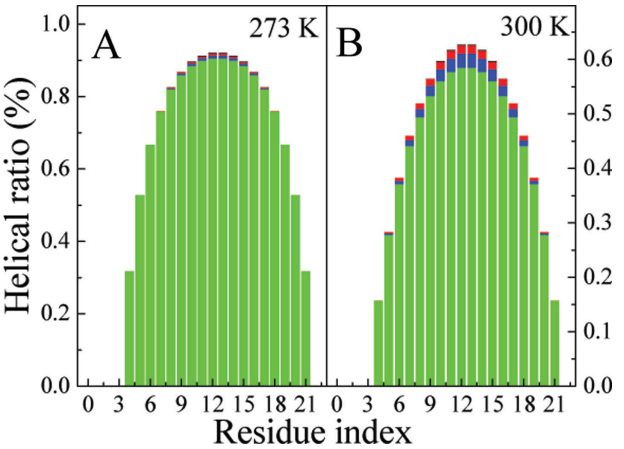

FIGURE 4 Distribution of probabilities for each residue being helical (hydrogen bonded) in the AP at 273 K (A), and 300 K (B) for $\mu = 1$ (green) $\mu = 2$ (blue), $\mu = 3$ (red) and $\mu = 4$ (black).

The general feature of the model are significantly higher helical probabilities for the central residues compared to the chain termini in agreement with numerous other statistical mechanical models for helix-coil transition[7,17,30] as well as experimental results.[39–41] In addition, Figure 4 shows that the helical probability of each individual residue in the chain increases with the increasing value of μ. This is especially evident from the plot of the residue helical probability distributions at 300 K (Figure 4B) and the most pronounced effect is observed for the residues near the center of the sequence. The residue-level helical probabilities of the oligopeptide are, therefore, dependent on the range of interactions considered in the ZB model. In other words, microscopic description of the helix-coil transition varies with μ, despite the fact that all models, independently of μ, fit the global helix-coil transition according to the CD and FTIR experimental data.

Free Energy Surfaces for the Helix-Coil Transition

To compare the microscopic predictions of the ZB models with different μ in more detail, we computed the free energy surfaces with the number of helical residues as the reaction coordinate for the four variants of the model. Using Eqs. (6) and (7) along with the full matrix expressions (given in the Appendix), we were able to take into account any number of helical sequences of any length and compute the exact statistical weight of the chain and, therefore, the exact conformational free energy surfaces within the assumptions of the ZB model. Calculation of the free energy surfaces as a function of the number of helical residues yields the free-energy barrier separating the helix and coil states and allows prediction of helix-coil transition kinetics,[42,43] which can be approxi-

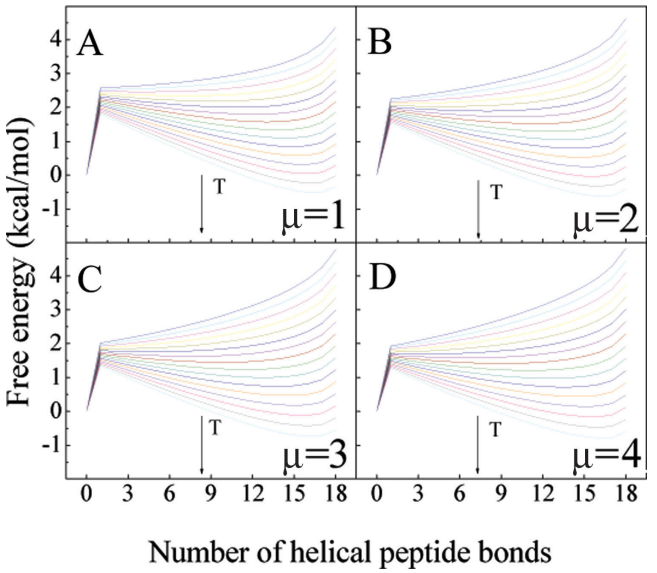

FIGURE 5 Free energy profiles as a function of the number of helical (hydrogen bonded) peptide bonds for ZB modes with $\mu = 1$ (A), $\mu = 2$ (B), $\mu = 3$ (C) and $\mu = 4$ (D). Temperature-dependent free energies are plotted from 273 K (light cyan curves) to 363 K (navy curves) every 5 K. Arrows indicate changes with decreasing temperature.

mately modeled as diffusion on the one-dimensional free energy surface.[44]

In Figure 5 we show the conformational free energies as a function of the number of helical residues, from 273 to 353 K with a temperature step of 5 K. In all cases the conformational free energy profile has two minima separated by a nucleation barrier indicative to the formation of the first hydrogen bond in the all-coil molecule.

While the plots in Figures 5A–5D look very similar, different values of μ in the ZB model produce observable differences in the calculated free energy surfaces. These differences are better visualized in Figure 6, where the probability distributions corresponding to the free energy surfaces from Figure 5 are plotted at 273 and 300 K. At 273 K all probability distributions have a maximum (corresponding to the free energy minimum) at 16 helical residues, which is the most probable number of helical residues in the sequence. Note, once again, that ZB model only allows 18 helical residues. However, even at 273 K it is clear that the distribution for $\mu = 1$ is narrower with a sharper maximum and more bimodal, that is the population of the all-coil configurations also increases. At 300 K the distributions for larger μ values become appreciably broader, populating more the states with very few formed hydrogen bonds. These apparently broader distributions of the helical states for the ZB model with larger μ are a consequence of lower nucleation free-energy barrier resulting in a more gradual free energy profiles. The decrease in the height of the nucleation free-energy barrier follows from the increase in the nucleation parameter σ (Table I) with the increase in μ. The nucleation free-energy barriers for several temperatures are compared in Table III.

The variations in the predicted free energy surfaces underline the fact that different variants of the ZB model ($\mu = 1$, 2, 3, and 4), while fitting the same overall helix-coil transition thermodynamics, yield different description of the helix-coil transition at the microscopic detail. The observed trends and potential significance of the observed differences among the tested variants of the ZB model are discussed in the next section.

DISCUSSION

Comparison of Zimm–Bragg Model Variants with Different μ

As our results show, all variants of the ZB model that differ in the span of residue–residue interactions from the nearest-neighbor ($\mu = 1$) up to i, $i + 4$ ($\mu = 4$) produce equally good fit to the experimental temperature-dependent CD and FTIR data for the AP oligopeptide and therefore describe the macroscopic, average α-helical content. By contrast, the microscopic predictions at the level of individual residues of each ZB model variant are significantly different. These include the nucleation parameters σ, and residue enthalpy and entropy changes for the α-helix propagation, as well as probability distributions of being helical for individual residues and free energy surfaces as a function of the number of

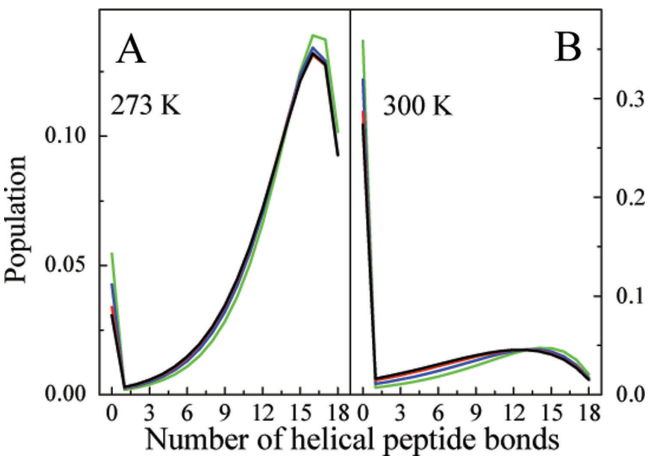

FIGURE 6 Distribution of populations of helical (hydrogen bonded) and coil (unbonded) states at 273 K (A) and 300 K (B) for ZB models $\mu = 1$ (green), $\mu = 2$ (blue), $\mu = 3$ (red) and $\mu = 4$ (black).

α-helical residues. All these properties show rather clear trends with increasing μ. The nucleation parameter increases with μ, as do (in the absolute value) the ΔH and ΔS for helix propagation (Table I). The probabilities of being helical for individual residues are higher for larger μ (see Figure 4), whereas the free energy surfaces exhibit lower nucleation barriers (see Figure 5) and result in broader distributions of helical populations that are shifted toward lower number of the helical residues for greater μ (see Figure 6).

These effects can be understood on the basis on Zimm–Bragg postulates, namely postulate (4): "the quantity zero for every bonded residue that follows a number of unbonded residues less than μ". This, in fact, is the postulate that defines how the long-range interactions are accounted for and differentiates between the variants of the ZB model with different μ.[10] As a consequence, the larger the μ, the smaller the number of configurations with a nontrivial contribution to the statistical weight in the partition function. For example, the ZB model with $\mu = 4$ does not allow any configurations of the chain with the stretches of three or less unbonded (coil) residues. Since this eliminates all sequences, where stretches of hydrogen-bonded segments are interleaved by short ($<\mu$) stretches of unbonded segments, this assumption inherently builds more cooperativity into models with higher μ.

On the other hand, the cooperativity of the helix-coil transition is strongly dependent on the value of the nucleation parameter σ—the smaller the σ, the more "cooperative" (sharper) the transition. This is demonstrated by distributions of the helix and coil populations that are sharper and shifted more toward higher fractions of hydrogen-bonded residues for smaller μ as a result of the decrease in σ (see Figure 6).

In the ZB model, the parameters μ and σ are effective values that approximate the dependence of σ on the number of unbonded residues before the first bonded one. The σ parameter is expected to increase with increasing μ[10] presumably because more "coil" (unbonded) residues before the first one to hydrogen bond represent smaller conformational restriction than those already hydrogen bonded within the preceding α-helical stretch. The increase in σ with μ can also be understood on the basis of the reduced statistical contribution of the partially helical configurations with increasing μ. Greater value of σ facilitates the formation of shorter α-helical stretches and counteracts the loss of the "forbidden" partially helical states.

Similar arguments can explain the trends in ΔH and ΔS, the enthalpy and entropy, respectively, required for adding a helical residue to the pre-existing sequence of helical residues. Both ΔH and ΔS increase in their absolute value with the increasing μ (Table I). This is, once again, due to the fact that increasing μ results in reduced number of partially helical conformations, which contribute both the enthalpy and entropy to the partition function. Fewer allowed configurations for larger μ result in higher ΔH and ΔS per added residue to produce the same overall transition. The increase in ΔH and ΔS is also consistent with the purpose of higher μ to approximate the long-range interactions between the residues composing the chain. Longer span of the interresidue interactions translates into the increase in enthalpy resulting from adding the helical residue to the chain, which, on the other hand, must be counterbalanced by the increase in the (unfavorable) entropy change.

Just as the increase in the nucleation parameter and (in the absolute value) the enthalpy and entropy changes per residue in the helix-coil transition, the higher overall probabilities for the individual residues to be helical follow from larger μ. Since fewer hydrogen bonded segments contribute to the overall fraction of the α-helix, the probability of being helical for the individual residue must be greater to produce the same overall fractional helicity. To illustrate this fact more quantitatively, we rewrite Eq. (3) as:

$$p_{i,l} = [a_{i,l} \cdot b_{i,l}/(a_{i,l}b_{i,l} + x)] \tag{10}$$

where the Q is expressed as the sum of $b_{i,l} \cdot a_{i,l}$, the statistical weights corresponding to the residue i held helical, and the term x which is the statistical weight of the remaining configurations of the chain, corresponding to the residue i held coil. The three terms, $p_{i,l}$, $a_{i,l} \cdot b_{i,l}$, and x are functions of μ. The behavior of $p_{i,l}$ with respect to μ can be inferred from the analysis of the partial derivative of $p_{i,l}$ with respect to μ, $\partial(p_{i,l})_\mu$:

$$\partial(p_{i,l})_\mu = \frac{(a_{i,l} \cdot b_{i,l} + x) \cdot \partial(a_{i,l} \cdot b_{i,l})_\mu - a_{i,l} \cdot b_{i,l} \cdot \partial(a_{i,l} \cdot b_{i,l} + x)_\mu}{(a_{i,l} \cdot b_{i,l} + x)^2} = \frac{x \cdot \partial(a_{i,l} \cdot b_{i,l})_\mu - a_{i,l} \cdot b_{i,l} \cdot \partial(x)_\mu}{(a_{i,l} \cdot b_{i,l} + x)^2} \tag{11}$$

Since $(a_{i,l} \cdot b_{i,l} + x)^2$ is always positive, $\partial(p_{i,l})_\mu$ will be positive—and therefore $p_{i,l}$ will increase, if $x > \frac{a_{i,l} \cdot b_{i,l} \cdot \partial(x)_\mu}{\partial(a_{i,l} \cdot b_{i,l})_\mu}$. The higher the value of μ, the lower the increment of the statistical weights, because with each increment of μ, there will be an increased number of configurations of a statistical weight zero, due to the fourth assumption of the model. The consequences of this assumption are intensified in short peptides; in fact, in the limit $\mu = n - 3$, all possible configurations of x are assigned statistical weights of zero,

but the all-coil configuration, whose statistical weight is one. Therefore, with increase in μ, there is lower dependence of the statistical weight of x on μ. In the extreme case of x independent on μ, the derivative $\partial(p_{i,l})_\mu$ reduces to $x \cdot \partial(a_{i,l} \cdot b_{i,l})/(a_{i,l} \cdot b_{i,l} + x)^2$ and the condition $\partial(p_{i,l})_\mu > 0$ becomes $\partial(a_{i,l} \cdot b_{i,l})_\mu > 0$, since $x > 0$. But $\partial(a_{i,l} \cdot b_{i,l})_\mu > 0$ is always true, because the increased number of residues per segment (when increasing μ), implies an increased statistical weight of the configurations in the chain with the i residue held helical.

All four variants of the ZB model equally well fit the CD and FTIR experimental data, even though the microscopic predictions for the distributions of the helical probabilities among the individual residues differ. Since CD and FTIR provide global information about average α-helical content, but cannot sense the helical content for individual residues or even short segments of the chain, by using these traditional methods it is impossible to distinguish which variant of the model gives more realistic predictions. However, site-specific experimental techniques, such as ^{13}C isotopically edited IR[45–49] Raman[41,50] and vibrational CD (VCD),[40] and NMR[51,52] can provide data on the helix or coil state of a particular segment or residue in the sequence. Analysis of such site-specific thermal unfolding data could therefore offer more detailed insights into the microscopic nature of the helix-coil transition as well as performance of various statistical mechanical models.

Furthermore, kinetic measurements of helix-coil transition using laser temperature-jump methodology,[23,46,47,53] yield the rate constants, which can be related to the nucleation and propagation parameters[42,43] or, alternatively, to the height of the free-energy barrier separating the coil and helical states (see Figure 5). In principle, kinetics could therefore be used to distinguish which model provides the best description. In practice, however, the analysis of helix-coil transition kinetics introduces additional unknowns, in particular the rate constant (or constants) for the helix-coil interconversion of the individual segments,[43] which are also necessary for obtaining the absolute free-energy barrier heights. Since the helix-coil transition rates are also dependent on other factors, such as solvent viscosity,[54] it may be difficult to characterize the free-energy barriers with accuracy on the order of a kcal mol^{-1} using kinetic measurements alone. On the other hand, more light could be shed on these "hidden" properties of the free-energy surfaces by the combination of the fast kinetic experiments with site-specific probes, including ^{13}C-edited FTIR[46,47] or Raman studies on peptides with deuterated $C^{\alpha\text{-}H}$ groups.[41,50] Analyses of such experiments still remain to be done with models that take into account long-range intrahelical interactions, such as ZB models with $\mu > 1$ presented in this study.

The Zimm–Bragg Model Parameters

Since the ZB model parameters are important measures of helix forming tendencies, their determination for individual amino acids has been the focus of numerous studies and several experimental approaches have been developed.[5,8] Depending on the particular approach, the thermodynamic parameters describing the helix-coil transition can vary dramatically. In particular, the helix forming propensity of L-Ala amino acid remains controversial.

The discovery of stable helical structures in short alanine-rich oligopeptides by Baldwin and coworkers,[4] has been attributed to a very strong tendency of L-Ala to form α-helices. The α-helical propensity is most commonly measured by the ZB propagation factor s [Eq. (1)]. From analysis of the alanine-rich oligopeptide data, the s for L-Ala is near 1.5 at 273 K.[30] The residue enthalpy for L-Ala is calculated[28,30,33] near -1 kcal mol^{-1} res^{-1} with the nucleation parameter at 2–3 $\times$ 10^{-3}.[5,28] Not surprisingly, since similar oligopeptide model is used in this study, our ZB parameters (Tables I and II) correspond very well to these values. A different approach of Goch et al.,[33] using prenucleated short Ala sequences, also yielded very similar enthalpy parameters and helix propensities.

The above values are, however, in sharp contrast with the earlier experiments using the triblock[34] and host–guest random[35] copolymers. These approaches yield significantly lower helical propensities for L-Ala, about 1.08 at 273 K and close to 1.00 at 335 K.[8] The L-Ala residue enthalpies and corresponding nucleation parameters are also much lower: the triblock copolymer experiments[34] yield the enthalpy of -190 ± 40 cal mol^{-1} res^{-1} and the nucleation parameter of 1.4 $\times$ 10^{-4}, in good agreement with the values of -242 ± 21 cal mol^{-1} res^{-1} for the L-Ala enthalpy and the nucleation parameter of 8 $\times$ 10^{-4} determined from the host–guest random copolymers.[35] Furthermore, using synthetic helix-nucleating template, Kemp et al.[55] also obtained similar results.

The explanation for this discrepancy is likely in the presence of charged (or polar) residues, which are necessary to ensure solubility of the alanine-rich peptides. Kemp and coworkers,[36] and Vila et al.[37,38] investigated the effects of charged lysine residues on the helical content in alanine-rich peptides. The lysine significantly promotes the helical structure, which has been attributed to the shielding of the amide backbone hydrogen bonds from solvent by the charged lysine side chains, effectively having the same effect as reducing the

solvent polarity.[38] As a consequence, the backbone hydrogen bond stability increases substantially, resulting in a much higher apparent stability of the α-helix. The simulations of Vila et al.[38] bear this out by predicting >50% helicity in the Ala-Lys sequences, but only 6–12% in an all-Ala peptide, in agreement with very low helical content found experimentally by the host–guest studies.[34] Presumably, similar arguments can rationalize the results of Goch et al.[33] as the charged amino acids in the helix-nucleating metal-binding loop likely influence the solvation of the amide groups within the short alanine helix.

The ZB parameters reported here must therefore be regarded as effective values, which depend on the context of the peptide sequence.[18] In particular, the parameters implicitly factor in the competition for solvent between the peptide backbone and charged Arg side chains, which, in the light of the earlier discussion, are expected to have the dominant effect on the α-helix stability. In addition, the parameters include different helix forming tendencies of Ala and Arg residues, although helical propensity of Arg is only slightly smaller than that of Ala and both have similar temperature dependence.[8,30] Finally, as discussed in detail in the previous section, the values of the thermodynamic parameters (Table I) are "effective" in the sense that they depend on the details of model. Even for the same model peptide sequence and experimental data set, the resulting helix-coil transition parameters reflect the approximations and limitations of the particular model used in the analysis.

Limitations of the Zimm–Bragg Model

The limitations of the simple statistical mechanical models for helix-coil transitions have been discussed in detail[6,9,12] and several were also alluded to in the earlier discussion. An obvious limitation is the restriction of the model to a homopolymer. The stabilization of the helix is assumed to arise only from the amide hydrogen bonds and is considered the same regardless of the nature of the particular amino acid. Any specific electrostatic and hydrophobic interactions or solvation effects that would arise from the heteropolymer sequence are neglected, or, strictly speaking, implicitly factored into the model parameters. A number of authors have augmented the ZB and other helix-coil transition models by additional terms to take specific interactions into account.[13–16] Wako et al.[18] explicitly considered specific interactions for all pairs of amino acids up to i, $i + 4$, and showed that these are important particularly if protein sequences are to be modeled. Although the model of Wako et al. is much more physically realistic than the ZB model, incorporating additional interactions introduces more parameters whose precise determination generally requires a substantial amount of experimental data. In their model, Wako et al. had to optimize 860 parameters, which was done using the experimental structures for 37 proteins.[18]

In the ZB model, the long-range interactions are taken into account in much simpler way, essentially following from postulate (4), which restricts the μ residues before the first hydrogen bond to be unbonded, otherwise the interactions are independent on the length of the helical stretch. As ZB discuss in the original article,[10] several σ parameters should be defined that would depend on the length of the unbonded stretch preceding the first hydrogen-bonded amide. The μ value in the ZB model and ban on the less than μ unbonded residues before the first hydrogen bonded one represent an effective approximation with a single nucleation parameter σ.[10] As we have shown, even within this simple approximation of the original ZB model with only three parameters for each particular μ, it is difficult to determine the parameter values and the optimum value of μ precisely, since all the variants of the model provide equally good fits to the experimental data.

Another weakness of the ZB model is that definition of the state of the chain solely by hydrogen bonded states of the amide oxygen atoms may lead to somewhat unrealistic picture of the helical conformation. The first hydrogen bond is formed after μ (or more) unbonded residues, but since the hydrogen bond is always formed with the amino group of the third preceding residue, this implies that the three residues preceding the first one considered bonded have to make a helical turn. If counted by conformation (i.e., ϕ, ψ angles) for $\mu > 3$ there would additional three helical residues in each stretch, however for $\mu \leq 3$ the state of the chain becomes difficult to visualize, since some "coil" residues would necessarily be a part of the helical stretch. In this light, it seems reasonable to assign the statistical weight zero to every bonded residue that follows less than μ unbonded residues and consider $\mu > 3$, even though this may drastically underestimate the entropy of the chain by neglecting a large number of possible chain configurations. By not allowing "coil" stretches of less than μ residues, this assumption notably affects the residue helical probabilities and is the principal reason for the substantial differences in the microscopic predictions of the models, as discussed earlier.

Another direct consequence of counting only hydrogen bonds on the oxygens is that the first three residues of the chain (in this formulation from the C terminus) are always assigned a coil conformation (unbonded), because they cannot make hydrogen bonds on the amide oxygen. This makes

the chain "non-symmetric": the first three residues from the C-terminus are always unbonded, but the same is not true for the N-terminus. Although the helicity distribution along the peptide sequence is not expected to be symmetric,[51] the first three C-terminal residues are not always "coil". If one defined, by analogy, the state of the chain by hydrogen bonding of the amide N—H, it would be precisely the opposite.[6] Finally we note that the statistical counting poses a problem only for relatively short sequences; in the original calculations by ZB for very long polypeptides the state of the first three residues becomes insignificant.[10]

CONCLUSION

We have investigated the thermodynamics of the helix-coil transition in an alanine 21-mer oligopeptide using four variants of the ZB model from the nearest-neighbor ($\mu = 1$) to fourth nearest-neighbor ($\mu = 4$). The experimental CD and FTIR data were analyzed by SVD and global fitting to the ZB model, for which the partition functions were enumerated exactly for any number of helical segments (stretches) within the sequence. We have also calculated the (microscopic) residue helicity distributions and free energy surfaces as a function of the number of helical residues. All variants of the model are capable of fitting the experimental CD and FTIR data equally well. However, the microscopic helical probability distributions, the free energy surfaces, as well as the ZB model parameters (σ and s) differ as a consequence of varying the range of intrahelical interactions. The nearest-neighbor ZB model yields the most cooperative overall transition characterized by sharpest helix and coil probability distributions and highest nucleation free-energy barrier. With increasing μ, the contribution of states with less helical content becomes more significant. On the other hand, the probability of each individual residue to be helical increases with increase in μ, as do the residue enthalpy and entropy changes associated with the helix-coil transition, as well as the nucleation parameters. This appears to be a consequence of ZB postulates, which build more inherent cooperativity into the variants of the model with higher μ, which is in turn counterbalanced by larger nucleation parameter σ and, therefore, apparently less cooperative transition. The experimental data that provide only information on the average helical content, such as CD and FTIR are insufficient for distinguishing which variant of the ZB model performs better. Site-specific experimental studies, such as using isotopically edited vibrational spectroscopies or NMR, will be necessary to test the microscopic predictions of the different ZB model variants.

APPENDIX

The forms of the statistical weight matrices for Zimm–Bragg model with different μ are:

$$\begin{pmatrix} 1 & 1 \\ \sigma s & s \end{pmatrix} \text{for } \mu = 1, \quad \begin{pmatrix} 1 & 0 & 1 & 0 \\ \sigma s & 0 & 0 & 0 \\ 0 & 1 & 0 & 1 \\ 0 & s & 0 & s \end{pmatrix} \textit{for } \mu = 2,$$

$$\begin{pmatrix} 1 & 0 & 0 & 0 & 1 & 0 & 0 & 0 \\ \sigma s & 0 & 0 & 0 & 0 & 0 & 0 & 0 \\ 0 & 1 & 0 & 0 & 0 & 1 & 0 & 0 \\ 0 & s & 0 & 0 & 0 & s & 0 & 0 \\ 0 & 0 & 1 & 0 & 0 & 0 & 1 & 0 \\ 0 & 0 & 0 & 0 & 0 & 0 & 0 & 0 \\ 0 & 0 & 0 & 1 & 0 & 0 & 0 & 1 \\ 0 & 0 & 0 & s & 0 & 0 & 0 & s \end{pmatrix} \text{for } \mu = 3 \text{ and}$$

$$\begin{pmatrix} 1 & 0 & 0 & 0 & 0 & 0 & 0 & 0 & 1 & 0 & 0 & 0 & 0 & 0 & 0 & 0 \\ \sigma s & 0 & 0 & 0 & 0 & 0 & 0 & 0 & 0 & 0 & 0 & 0 & 0 & 0 & 0 & 0 \\ 0 & 1 & 0 & 0 & 0 & 0 & 0 & 0 & 1 & 0 & 0 & 0 & 0 & 0 & 0 & 0 \\ 0 & s & 0 & 0 & 0 & 0 & 0 & 0 & s & 0 & 0 & 0 & 0 & 0 & 0 & 0 \\ 0 & 0 & 1 & 0 & 0 & 0 & 0 & 0 & 0 & 1 & 0 & 0 & 0 & 0 & 0 & 0 \\ 0 & 0 & 0 & 0 & 0 & 0 & 0 & 0 & 0 & 0 & 0 & 0 & 0 & 0 & 0 & 0 \\ 0 & 0 & 0 & 1 & 0 & 0 & 0 & 0 & 0 & 0 & 1 & 0 & 0 & 0 & 0 & 0 \\ 0 & 0 & 0 & s & 0 & 0 & 0 & s & 0 & 0 & 0 & s & 0 & 0 & 0 & 0 \\ 0 & 0 & 0 & 0 & 1 & 0 & 0 & 0 & 0 & 0 & 0 & 0 & 1 & 0 & 0 & 0 \\ 0 & 0 & 0 & 0 & 0 & 0 & 0 & 0 & 0 & 0 & 0 & 0 & 0 & 0 & 0 & 0 \\ 0 & 0 & 0 & 0 & 0 & 1 & 0 & 0 & 0 & 0 & 0 & 0 & 0 & 1 & 0 & 0 \\ 0 & 0 & 0 & 0 & 0 & s & 0 & 0 & 0 & 0 & 0 & 0 & 0 & s & 0 & 0 \\ 0 & 0 & 0 & 0 & 0 & 0 & 1 & 0 & 0 & 0 & 0 & 0 & 0 & 0 & 1 & 0 \\ 0 & 0 & 0 & 0 & 0 & 0 & 0 & 0 & 0 & 0 & 0 & 0 & 0 & 0 & 0 & 0 \\ 0 & 0 & 0 & 0 & 0 & 0 & 0 & 1 & 0 & 0 & 0 & 0 & 0 & 1 & 0 & 1 \\ 0 & 0 & 0 & 0 & 0 & 0 & 0 & s & 0 & 0 & 0 & 0 & 0 & 0 & s & \end{pmatrix} \text{for } \mu = 4.$$

REFERENCES

1. Doty, P.; Holtzer, A. M.; Bradbury, J. H.; Blout, E. R. J Am Chem Soc 1954, 76, 4493–4494.
2. Blout, E. R.; Karlson, R. H. J Am Chem Soc 1958, 80, 1259–1260.
3. Poland, D.; Scheraga, H. A. Theory of Helix-Coil Transition in Biopolymers; Academic Press: New York, 1970.
4. Marqusee, S.; Robbins, V. H.; Baldwin, R. L. Proc Natl Acad Sci USA 1989, 86, 5286–5290.
5. Scholtz, J. M.; Baldwin, R. L. Annu Rev Biophys Biomol Struct 1992, 21, 95–118.
6. Qian, H.; Schellman, J. A. J Phys Chem 1992, 96, 3987–3994.
7. Muñoz, V.; Serrano, L. Struct Biol 1994, 1, 399–409.

8. Scheraga, H. A.; Vila, J. A.; Ripoll, D. R. Biophys Chem 2002, 101, 255–265.
9. Doig, A. J. Biophys Chem 2002, 101, 281–293.
10. Zimm, B. H.; Bragg, J. K. J Chem Phys 1959, 31, 526–535.
11. Cantor, C. R.; Schimmel, P. R. Biophysical Chemistry. III. The Behavior of Biological Macromolecules; W. H. Freeman: New York, 1980.
12. Saroff, H. A.; Kiefer, J. E. Biopolymers 1999, 49, 425–440.
13. Vasquez, M.; Scheraga, H. A. Biopolymers 1988, 27, 41–58.
14. Gans, P. J.; Lyu, P. C.; Manning, M. C.; Woody, R. W.; Kallenbach, N. R. Biopolymers 1991, 31, 1605–1614.
15. Robert, C. H. Biopolymers 1990, 30, 335–347.
16. Finkelstein, A. V.; Badretdinov, A. Y.; Ptitsyn, O. B. Protein Struct Funct Genet 1991, 10, 287–299.
17. Andersen, N. H.; Tong, H. Protein Sci 1997, 6, 1920–1936.
18. Wako, H.; Saito, N.; Scheraga, H. A. J Protein Chem 1983, 2, 221–249.
19. Wako, H.; Saito, N. J Phys Soc Jpn 1978, 44, 1931–1938.
20. Wako, H.; Saito, N. J Phys Soc Jpn 1978, 44, 1939–1945.
21. Bruscolini, P.; Pelizzola, A. Phys Rev Lett 2002, 88, 1–4.
22. Henry, E. R.; Hofricheter, J. Methods Enzymol 1992, 210, 129–192.
23. Williams, S.; Causgrove, T. P.; Gilmanshin, R.; Fang, K. S.; Callender, R. H.; Woodruff, W. H.; Dyer, R. B. Biochemistry 1996, 35, 691–697.
24. Yoder, G.; Pancoska, P.; Keiderling, T. A. Biochemistry 1997, 36, 15123–15133.
25. Huang, C.-Y.; Klemke, J. W.; Getahun, Z.; DeGrado, W F.; Gai, F. J Am Chem Soc 2001, 123, 9235–9238.
26. Rialdi, G.; Hermans, J. J Am Chem Soc 1966, 88, 5719–5720.
27. Chou, P. Y.; Scheraga, H. A. Biopolymers 1971, 10, 657–680.
28. Scholtz, J. M.; Qian, H.; York, E. J.; Stewart, J. M.; Baldwin, R. L. Biopolymers 1991, 31, 1463–1470.
29. Scholtz, J. M.; Marqusee, S.; Baldwin, R. L.; York, E. J.; Stewart, J. M.; Santoro, M.; Bolen, D. W. Proc Natl Acad Sci USA 1991, 88, 2854–2858.
30. Chakrabartty, A.; Kortemme, T.; Baldwin, R. L. Protein Sci 1994, 3, 843–852.
31. Yang, A. S.; Honig, B. J Mol Biol 1995, 252, 351–365.
32. Lopez, M. M.; Chin, D. H.; Baldwin, R. L.; Makhatadze, G. I. Proc Natl Acad Sci USA 2002, 99, 1298–1302.
33. Goch, G.; Maciejczyk, M.; Oleszczuk, M.; Stachowiak, D.; Malicka, J.; Bierzynski, A. Biochemistry 2003, 42, 6840–6847.
34. Ingwall, R. T.; Scheraga, H. A.; Lotan, N.; Berger, A.; Katchals, E. Biopolymers 1968, 6, 331–368.
35. Platzer, K. E. B.; Scheraga, H. A.; Andreatt, R. H.; Ananthan V S. Macromolecules 1972, 5, 177–187.
36. Williams, L.; Kather, K.; Kemp, D. S. J Am Chem Soc 1998, 120, 11033–11043.
37. Vila, J. A.; Ripoll, D. R.; Scheraga, H. A. Proc Natl Acad Sci USA 2000, 97, 13075–13079.
38. Vila, J. A.; Ripoll, D. R.; Scheraga, H. A. Biopolymers 2001, 58, 235–246.
39. Decatur, S. M. Biopolymers 2000, 54, 180–185.
40. Silva, R.; Kubelka, J.; Bour, P.; Decatur, S. M.; Keiderling, T. A. Proc Natl Acad Sci USA 2000, 97, 8318–8323.
41. Ianoul, A.; Mikhonin, A.; Lednev, I. K.; Asher, S. A. J Phys Chem A 2002, 106, 3621–3624.
42. Schwarz, G. J Mol Biol 1965, 11, 64–77.
43. Poland, D.; Scheraga, H. A. J Chem Phys 1966, 45, 2071–2090.
44. Doshi, U.; Muñoz, V. Chem Phys 2004, 307, 129–136.
45. Decatur, S. M.; Antonic, J. J Am Chem Soc 1999, 121, 11914–11915.
46. Huang, C. Y.; Getahun, Z.; Wang, T.; DeGrado, W. F.; Gai, F. J Am Chem Soc 2001, 123, 12111–12112.
47. Huang, C. Y.; Getahun, Z.; Zhu, Y. J.; Klemke, J. W.; DeGrado, W. F.; Gai, F. Proc Natl Acad Sci USA 2002, 99, 2788–2793.
48. Venyaminov, S. Y.; Hedstrom, J. F.; Prendergast, F. G. Protein Struct Funct Genet 2001, 45, 81–89.
49. Decatur, S. M. Acc Chem Res 2006, 39, 169–175.
50. Mikhonin, A. V.; Asher, S. A.; Bykov, S. V.; Murza, A. J Phys Chem B 2007, 111, 3280–3292.
51. Liff, M. I.; Lyu, P. C.; Kallenbach, N. R. J Am Chem Soc 1991, 113, 1014–1019.
52. Millhauser, G. L.; Stenland, C. J.; Bolin, K. A.; van deVen, F. J. M. J Biomol NMR 1996, 7, 331–334.
53. Thompson, P. A.; Eaton, W. A.; Hofrichter, J. Biochemistry 1997, 36, 9200–9210.
54. Jas, G. S.; Eaton, W. A.; Hofrichter, J. J Phys Chem B 2001, 105, 261–272.
55. Kemp, D. S.; Oslick, S. L.; Allen, T. J. J Am Chem Soc 1996, 118, 4249–4255.

Reviewing Editor: David Case